Received: 14 August 2022 | Revised: 17 September 2022 | Accepted: 27 September 2022

DOI: 10.1002/agt2.284

Aggregate Open Access WILEY

RESEARCH ARTICLE

Carrier-free nanodrugs for stemness inhibition-enhanced photodynamic therapy

Yuwei Liu[1,2,3] | **Kaiqi Long**[1,2,3] | **Tianyi Wang**[1,2,3] | **Weirong Kang**[1,2,3] | **Weiping Wang**[1,2,3]

[1]State Key Laboratory of Pharmaceutical Biotechnology, The University of Hong Kong, Hong Kong, China

[2]Department of Pharmacology and Pharmacy, Li Ka Shing Faculty of Medicine, The University of Hong Kong, Hong Kong, China

[3]Laboratory of Molecular Engineering and Nanomedicine, Dr. Li Dak-Sum Research Centre, The University of Hong Kong, Hong Kong, China

Correspondence
Weiping Wang, State Key Laboratory of Pharmaceutical Biotechnology, The University of Hong Kong, Pokfulam, Hong Kong, China.
Email: wangwp@hku.hk

Funding information
Research Grants Council of Hong Kong, Grant/Award Number: 27115220; Ming Wai Lau Centre for Reparative Medicine Associate Member Program

Abstract

Cancer stem cell (CSC) has been considered a key driver of tumor growth, recurrence, and metastasis due to its self-renewal and tumor initiation capacities called stemness. Stemness is also responsible for the high resistance of CSC to current therapeutic strategies, including photodynamic therapy (PDT) and chemotherapy. In this study, a carrier-free nanodrug (designated as MKCe6 nanoparticle [NP]) self-assembled by photosensitizer chlorin e6 (Ce6) and stemness inhibitor MK-0752 was prepared for effective tumor repression. Stemness inhibition caused by MK-0752 could sensitize CSCs to PDT. Benefiting from the high drug-loading capacity and efficient cellular internalization, MKCe6 NPs exhibited good performance in PDT and stemness inhibition. In this way, effective tumor growth repression and tumorigenesis inhibition by MKCe6 NPs were observed both in vitro and in vivo. This self-delivery nanodrug for stemness inhibition-enhanced photodynamic therapy may provide new insights for clinical cancer therapy.

KEYWORDS

cancer stemness, nanomedicine, Notch pathway, photodynamic therapy, self-assembly

1 | INTRODUCTION

Cancer stem cells (CSCs), which are also known as cancer stem-like cells, represent a small proportion of tumor cells that are decisive factors accounting for intratumor heterogeneity.[1–3] As undifferentiated cells, CSCs retain the ability of self-renewal and differentiation, through which CSCs exert their tumorigenic potential, leading to tumor recurrence and metastasis.[4–6] Besides, CSCs exhibit inherent resistance to current therapeutic strategies like chemotherapy,[7] radiotherapy,[8] and photodynamic therapy (PDT).[9] Though those differentiated cancer cells can be killed by the above-mentioned therapy, a small subpopulation of the resistant cells (mainly CSCs) still manage to survive, and finally drive tumor relapse.[10–12] As evidenced from clinical studies, a rise in the CSC proportion after anticancer therapy indicates a worse prognosis in cancer patients.[13,14]

Notch signaling pathway is one of the activated signal pathways during tumor progression.[15,16] Subsequent studies have verified that the Notch signaling pathway plays a vital role in regulating the differentiation and self-renewal of CSCs,[17–19] indicating that Notch is a therapeutic target for stemness regulation. For cancer therapy, Notch pathway inhibitors have been used to sensitize CSCs to chemotherapy or radiation therapy, enabling better therapeutic efficacy.[20,21]

PDT is a promising spatiotemporally controllable treatment, which has been approved for clinical cancer therapy.[22–24] PDT can efficiently kill cancer cells by generating toxic reactive oxygen species (ROS) at tumor lesions. However, the efficacy of PDT can be undermined by the presence of CSCs,[25,26] which exhibit high resistance toward ROS.[27] Therefore, we hypothesized that eliminating CSCs in tumors during PDT treatment may be a promising approach for tumor eradication.

Combination of Notch pathway deactivation and PDT will not only kill differentiated cancer cells but also sensitize resistant CSCs to PDT, resulting in whole tumor ablation with less recurrence. Herein, a carrier-free nanodrug system combining Notch pathway inhibition and PDT was developed via the co-assembly of two molecules, chlorin e6 (Ce6) and MK-0752. MK-0752 is a γ-secretase inhibitor that can specifically inhibit Notch pathway (Notch1, Notch2, Notch3, Notch4) for

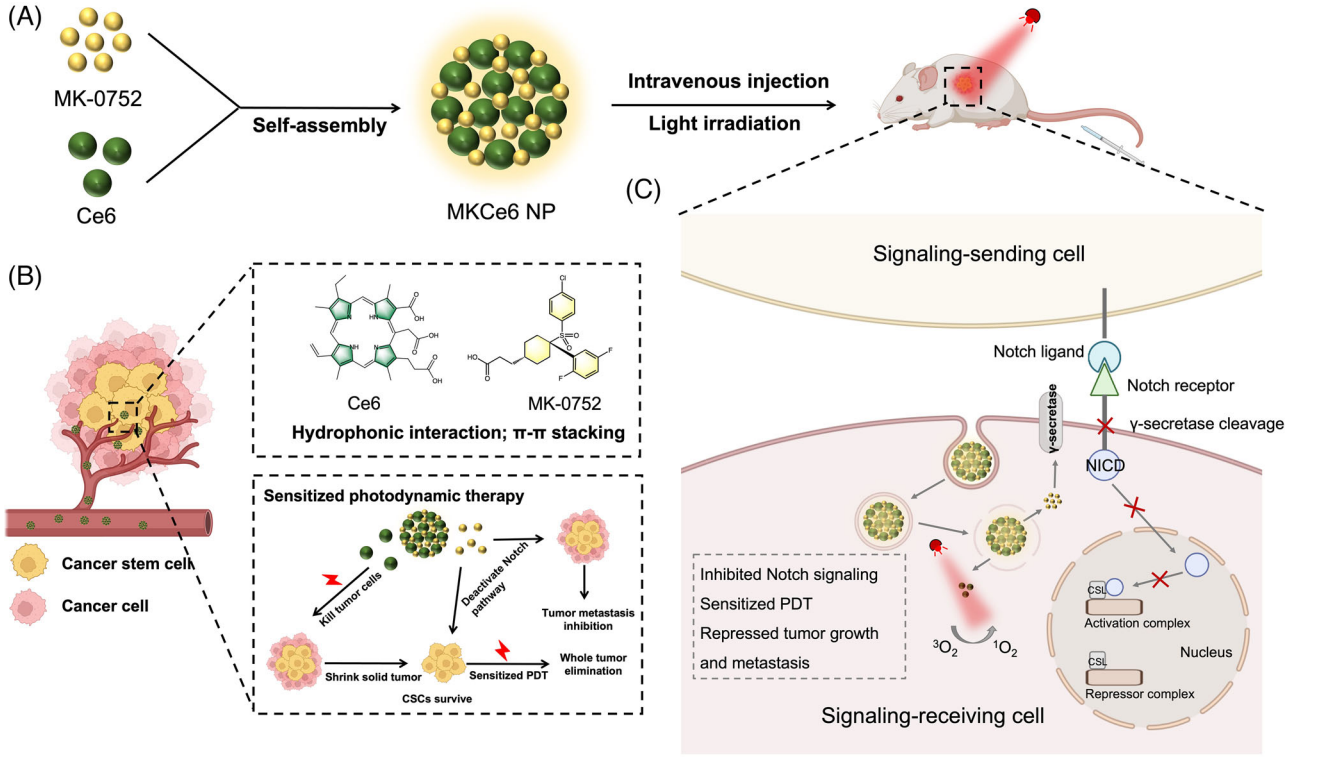

SCHEME 1 Schematic illustration of stemness inhibition-enhanced photodynamic therapy (PDT) with MKCe6 nanoparticles (NPs). (A) Self-assembly of Ce6 and MK-0752 into MKCe6 NPs. (B) Therapeutic effects of MKCe6 NPs in tumor growth inhibition. PDT effect of Ce6 can kill tumor cells and shrink solid tumor, while MK-0752 inhibits Notch pathway to inhibit cancer stemness, sensitize cancer stem cells (CSCs) to PDT, and inhibit tumor cells metastasis. (C) The molecular mechanisms of PDT effect and inhibition of Notch pathway by MKCe6 NPs in tumor cells. CSL (CBF1, Suppressor of Hairless, Lag-1) is a transcription factor that is responsible for activating the gene downstream of the Notch signaling pathway, NICD (Notch intracellular domain)

stemness inhibition by blocking the cleavage of γ-secretase and the release of Notch intracellular domain (NICD).[28,29] Ce6 is an FDA-approved photosensitizer with high quantum yield of ROS upon light irradiation and good biocompatibility for PDT.[30–32] In this study, Ce6 and MK-0752 can self-assemble into stable and spherical nanoparticles (MKCe6 NPs) at optimized ratio without extra excipient by virtue of π−π stacking and hydrophobic interactions. Furthermore, stemness inhibition caused by MK-0752 can sensitize CSCs to PDT. MKCe6 NPs exhibit both high drug-loading capacity and efficient cellular internalization capability. After systemic administration, the NPs can accumulate in tumor tissues through the enhanced permeability and retention (EPR) effect and effectively block the Notch signaling to inhibit cancer stemness. Moreover, stemness inhibition sensitized CSCs to PDT with near-infrared (NIR) light irradiation (Scheme 1). As a result, the combination of PDT and Notch pathway inhibition by MKCe6 NPs significantly repressed tumor growth and stifled the possibility of tumor recurrence and metastasis, while no obvious side effects were observed. To our knowledge, it is the first demonstration of combining PDT with Notch pathway regulation for combating solid tumors.

2 | RESULTS AND DISCUSSION

2.1 | Preparation and characterization of MKCe6 NPs

MKCe6 NPs were fabricated by a simple flash nanoprecipitation approach with Ce6 and MK-0752. It is worth noting that the key parameters of the NPs could be influenced by the feeding ratio of Ce6 to MK-0752. NPs with different feeding ratios exhibited consistent spherical morphology, which were visualized by transmission electron microscopy (TEM; Figure 1A). However, their particle size, polydispersity index (PDI), and stability varied (Figure 1B,C). NPs with the molar ratio of 1:4 showed the best stability within 5 days as well as the lowest PDI value. Hence, the molar ratio of 1:4 of Ce6 to MK-0752 was chosen as an optimal ratio for further study. The drug-loading capacity and encapsulation efficiency were calculated according to the standard curves of Ce6 and MK-0752 (Figures S1 and S2). Particularly, the NPs were measured as 168.4 nm in size and −24.1 mV for zeta potential (Figure 1D), which could utilize the EPR effect for tumor accumulation.[33,34] Notably, the NPs obtained at the feed ratio of 1:4 also had a narrow size distribution and exhibited good stability under physiological condition (Figure S3), which were of advantage for antitumor drugs to exert their therapeutic functions. Moreover, the size value and PDI of solutions/suspensions of MK-0752, Ce6, or simple mixture of Ce6 and MK-0752 are big as characterized by dynamic light scattering (DLS), implying that pure MK-0752, pure Ce6, and a simple mixture of Ce6 and MK-0752 cannot form well-dispersed and stable NPs (Figure S4).

Next, the self-assembly mechanism of MKCe6 NPs was investigated by spectroscopy study. MKCe6 NPs exhibit absorption peaks at 405 and 640 nm (peaks of Ce6) and 280 nm (peak of MK-0752) (Figure 1E), indicating the successful co-assembly of the two molecules into NPs. Free Ce6 forms big aggregates in water due to its hydrophobicity, while it can be dissolved in methanol. Compared with

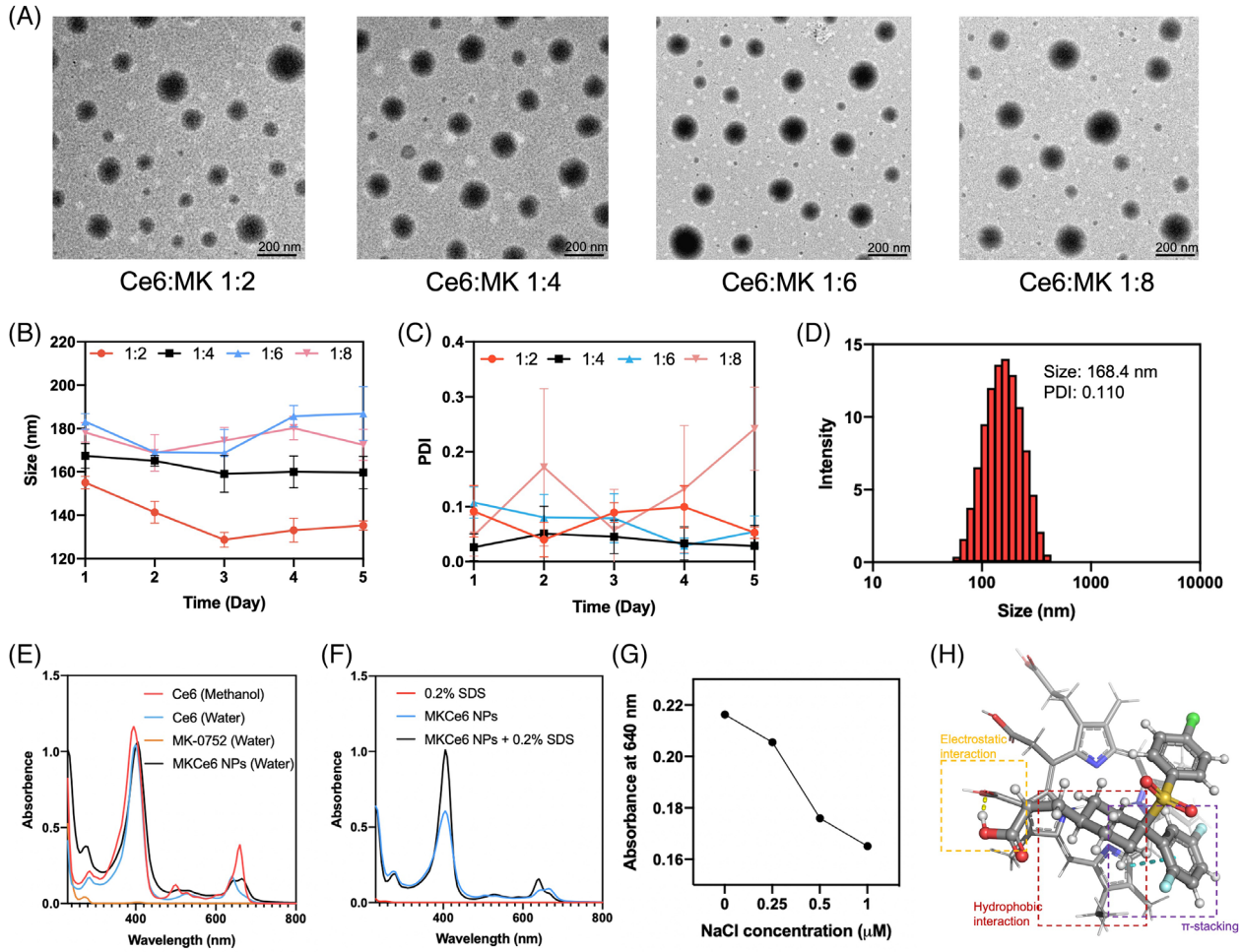

FIGURE 1 Preparation and characterizations of MKCe6 nanoparticles (NPs). (A) Transmission electron microscopy (TEM) images of NPs self-assembled by Ce6 and MK-0752 at the molar ratios of 1:2, 1:4, 1:6, and 1:8. (B) Hydrodynamic sizes and (C) polydispersity index (PDI) values of MKCe6 NPs at various feeding ratios in 5 days. Data were presented as mean ± SD (n = 3). (D) Size distribution of MKCe6 NPs at the molar ratio of 1:4 characterized by dynamic light scattering (DLS). (E) Ultraviolet (UV)-Vis absorption spectra of MKCe6 NPs, Ce6, and MK-0752 in the presence of water or methanol. (F) UV-Vis absorption spectra of MKCe6 NPs in the presence of sodium dodecyl sulfate (SDS) (0.2%, w/v). (G) Absorbance change of MKCe6 NPs in the presence of different concentrations of NaCl solutions at 640 nm. (H) Schematic illustration of the self-assembly of Ce6 and MK-0752 through hydrophobic interaction, $\pi-\pi$ stacking, and electrostatic interaction, which is analyzed by molecular docking

free Ce6 in water, weakened red-shifted absorption peaks were observed in MKCe6 NPs, indicating molecular interactions between Ce6 and MK-0752 resulted in the formation of NPs from two molecules.[35] The pyrrole groups of Ce6 and the aromatic structure of MK-0752 can form $\pi-\pi$ stacking of two molecules. With the addition of sodium dodecyl sulfate (SDS) (Figure 1F), the absorption peaks of MKCe6 NPs were significantly decreased, which indicates the hydrophobic interaction-based self-assembly of MKCe6 NPs. With the addition of sodium chloride (Figure 1G), the turbidity of the NP solution decreased, indicating that the increase of ionic strength triggered the NPs to disintegrate. The potential interaction sites between Ce6 and MK-0752 were simulated using molecular docking analysis (Figure 1H). To conclude, MKCe6 NPs were self-assembled by the combination of hydrophobic interaction, $\pi-\pi$ stacking, and electrostatic interaction.

2.2 | Internalization of MKCe6 NPs in cells

To test the cell internalization of MKCe6 NPs, Ce6 was utilized as an indicator to track the NPs in vitro. HCT116 cells were incubated with free Ce6 and MKCe6 NPs, separately, for confocal laser scanning microscopy (CLSM) imaging (Figure 2A). With the increase of incubation time, the red fluorescence representing Ce6 gradually strengthened. Notably, compared with free Ce6, MKCe6 NPs showed significantly intensified fluorescence, which indicates that MKCe6 NPs exhibit higher cellular uptake efficiency. Next, flow cytometry was performed to quantify the intracellular Ce6. As shown in Figure 2B and Figure S5, the relative fluorescence intensity of MKCe6 NPs was nearly twofold higher than that of free Ce6, providing further support for the efficient cellular internalization of MKCe6 NPs. The distinct difference in cellular uptake might be ascribed to the efficient endocytosis pathway in the cellular internalization of NPs, demonstrating the advantage of nanoplatforms in drug delivery.[36]

2.3 | PDT effect of MKCe6 NPs in vitro

The generation of singlet oxygen ($^1O_2$) by MKCe6 NPs was measured by the fluorescence spectrum using SOSG (Singlet Oxygen Sensor Green®) as an indicator. The result

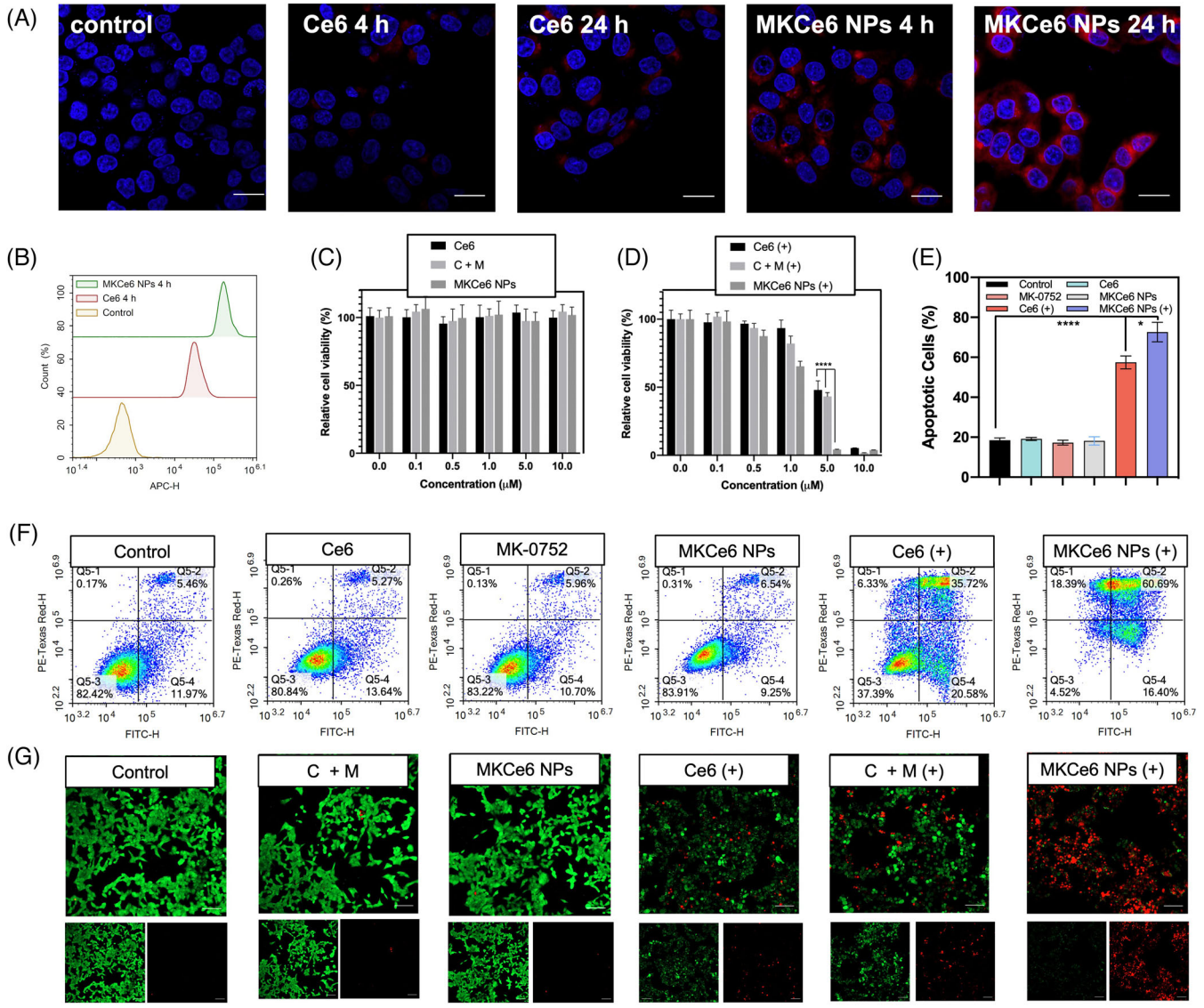

FIGURE 2 Cellular uptake and photodynamic therapy (PDT) effect of MKCe6 nanoparticles (NPs) in vitro. (A) Confocal laser scanning microscopy (CLSM) image of HCT116 cells after treatment with Ce6 or MKCe6 NPs at an equivalent concentration for 4 and 24 h. Scale bar: 50 μm. (B) Flow cytometry analysis of HCT116 cells incubated with Ce6 or MKCe6 NPs for 4 and 24 h. Cell viability of HCT116 cells after treatment with gradient concentrations of Ce6, MK-0752 plus Ce6, and MKCe6 NPs (C) in the absence or (D) in the presence of light irradiation (n = 5). (E) Quantitative apoptotic cell analysis and (F) flow cytometry of HCT116 cells after treatment with MK-0752, Ce6, and MKCe6 NPs in the absence or presence of light irradiation (n = 3). (G) Calcein AM (green fluorescence, indicating living cells) and PI (red fluorescence, indicating dead cells) staining of HCT116 cells after treatment with Ce6, MK-0752 plus Ce6, and MKCe6 NPs in the absence or presence of light irradiation. Scale bar: 50 μm. "(+)" represents the application of light irradiation. "C + M" represents the treatment of Ce6 plus MK-0752. Data were shown as mean ± SD. *p < 0.05, **p < 0.01, ***p < 0.001, ****p < 0.0001, and ns (not significant) were analyzed using Student's *t*-test

indicats the NPs can generate $^1O_2$ upon light irradiation in a time-dependent manner (Figure S6). Then the ROS generation of MKCe6 NPs in HCT116 cells was detected by CLSM using 2′,7′-dichlorodihydrofluorescein diacetate (DCFH-DA) as the sensor. As shown in Figure S7, negligible SOSG fluorescence was observed in the absence of Ce6 or light irradiation, suggesting weak ROS generation. However, cells treated with MKCe6 NPs and light irradiation exhibited strong green fluorescence, which was corroborated to increase with prolonged light irradiation. Of note, the fluorescence intensity of the MKCe6 NPs group was significantly stronger than that of free Ce6 or mixture of Ce6 plus MK-0752 due to the enhancement of cellular uptake of the NPs (Figure 2A). The excellent ROS generation led us to evaluate the antitumor efficacy of MKCe6 NPs in vitro. HCT116 cells were incubated with a gradient concentration of Ce6, mixture of Ce6 and MK-0752, and MKCe6 NPs, separately, for MTT assay. Owning to the low ROS generation efficiency, all the three groups exhibited weak toxicity without light irradiation, despite at relatively high concentrations (Figure 2C and Figure S8). However, once the light was applied, strong cytotoxicity against HCT116 was observed (Figure 2D). Particularly, the group treated with MKCe6 NPs exhibited the strongest photo-induced toxicity compared with other groups at certain concentrations, which was attributed to the enhanced ROS generating ability by virtue of better cellular uptake. Subsequently, the enhanced cytotoxicity of MKCe6 NPs was further verified by apoptosis assay and live/dead cell staining assay. Nearly 77% of HCT116 cells treated with MKCe6 NPs plus light irradiation were detected to be in early or late apoptosis conditions, which was significantly higher than other groups (Figure 2E,F). Consistent

results were observed in live/dead cell staining assay, where nearly all the cells treated with MKCe6 NPs plus light irradiation showed strong red fluorescence, demonstrating excellent antitumor activity (Figure 2G). In conclusion, MKCe6 NPs could enhance the PDT efficiency by virtue of efficient cellular internalization.

2.4 | In vitro stemness inhibition

The excellent cellular uptake and improved in vitro PDT effect of MKCe6 NPs encouraged us to explore whether such enhanced cell internalization would bring better stemness inhibition effect, given that stemness has been identified to play an important role in various treatment resistance including PDT.[26,37] HCT116 cells were incubated with free MK-0752 or MKCe6 NPs at different concentrations for 24 h. The western blot results showed that MKCe6 NPs exhibited more efficient Notch inhibition than free MK-0752, and such effect was in a concentration-dependent manner (Figure 3A and Figure S9). The deactivation of Notch signaling was confirmed by the downregulation of Notch1 as representative. Significant decrease in the expression of CD133, Oct4, and Sox2 was observed, which were identified as stemness markers.[38] Moreover, as a γ-secretase inhibitor, MK-0752 blocks the Notch signaling pathway by inhibiting γ-secretase cleavage and decreasing the expression of Notch intracellular domain protein (NICD) consequently.[39] To be noted, the expression of all stemness markers was the lowest in the cells treated with MKCe6 NPs due to the Notch inhibition effect. Oct4 and Sox2 are involved in the regulation of cancer stem cell self-renewal, maintenance of their stem cell characteristics, and resistance to traditional therapies.[40,41] Therefore, total mRNA of HCT116 cells were extracted and the gene expression of Oct4 and Sox2 were tested. As shown in Figure 3B,C, the mRNA expression of HCT116 cells was downregulated in a dose-dependent manner and the groups treated with MKCe6 NPs showed the lowest gene expression. The stemness inhibition of HCT116 cells was further visualized by capturing confocal images. CD133 is one of the characterized markers in colon CSCs, and Oct4 plays a critical role in maintaining stem cells.[42] These two markers were chosen as representatives for CLSM imaging. The results showed that the MK-0752 decreased the expression of CD133 and Oct4, while MKCe6 NPs exhibited the best inhibition effect by the virtue of improved cellular uptake (Figure S10).

The ability to form tumor spheres under serum-free conditions is regarded as an indicator of the proportion of stem cells.[43,44] HCT116 stem cells ($CD24^+CD44^+$) (Figure S11) were sorted out. The tumorsphere formation ability of the cells was evaluated after the treatment with free Ce6, free Ce6 plus MK-0752, or MKCe6 NPs.[45] As shown in Figure 3D,E, the group treated with free Ce6 still can form spheres in 24 h after light irradiation due to PDT resistance of stem cells. The group treated with free Ce6 plus MK-0752 formed spheres with smaller size due to reduced proportion of stem cells. The group treated with MKCe6 NPs exhibited the least sphere formation due to the efficient decrease in the proportion of CSCs.

To further confirm the PDT resistance of CSCs and stemness inhibition effect of the developed system, the Hoechst side population (SP) method was used to isolate cancer stem-like cells, which can easily form tumorspheres in serum-free medium and harbor a high percentage of $CD44^+CD24^+$ cell population (Figure S12). The sorted HCT116 SP cells showed resistance to PDT compared with normal HCT116 cells, indicating the CSCs were resistant to PDT (Figure 3F). However, they exhibited higher sensitivity to PDT after treatment with MK-0752 (Figure 3G), indicating cancer stemness inhibition can reverse PDT resistance. Besides, MKCe6 NPs displayed the highest cytotoxicity by virtue of enhanced cellular uptake of NPs and synergized therapeutic efficacy of two drug molecules (Figure 3H).

To conclude, MKCe6 NPs could improve the stemness inhibiting efficiency as reflected by the distinct downregulation of stemness markers and sphere formation suppression. Colon CSCs are resistant to PDT, while effective inhibition of Notch signaling can sensitize them to PDT.

2.5 | MKCe6 NPs inhibited HCT116 cell invasion and migration

CSCs are the culprit of cancer metastasis and postoperative relapse due to their strong invasion and migration ability. A wound healing experiment was performed to test the migration ability of HCT116 cells. The migration ability is reflected by the width of residual scars. Wider scarring indicates more significant inhibition of cell migration. As shown in Figure S13, free MK-0752 inhibited the cell migration in a dose-dependent manner. However, the migration inhibition effect of MK-0752 in the form of MKCe6 NPs was significantly enhanced. Collectively, MKCe6 NPs could efficiently reduce the metastatic potential of cancer cells by improved stemness inhibition.

Transwell® chamber assay was used with or without Matrigel to examine cancer cells' capability of migrating and invading through extracellular matrix. In the captured pictures (Figure S14 and 3I), the violet regions denote the cells that migrated or invaded. Accordingly, Ce6-mediated PDT mitigated the cell migration and invasion compared with the control group while the addition of MK-0752 enhanced such effects. Notably, cells treated with MKCe6 NPs exhibited much less migration and invasion, with the least cells passing through the chamber. Furthermore, a 3D-tumor sphere model was constructed to test the pharmacological functions of MKCe6 NPs (Figure S15). Compared with the control group, the group treated with Ce6 under light irradiation in second round showed less adherence ability, while the group treated with free Ce6 plus MK-0752 demonstrated diminished adherence ability in the first round of light irradiation. Notably, for the sphere treated with MKCe6 NPs, no adherence ability was observed with almost no tentacles growing in whole treatment processes.

2.6 | Tumor accumulation and antitumor efficacy of MKCe6 NPs in vivo

Ce6 was utilized as NIR fluorescent indicator for in vivo biodistribution analysis. The biodistribution of free Ce6 and MKCe6 NPs was assessed in an HCT116 xenograft mouse model. After Ce6 and MKCe6 NPs were intravenously

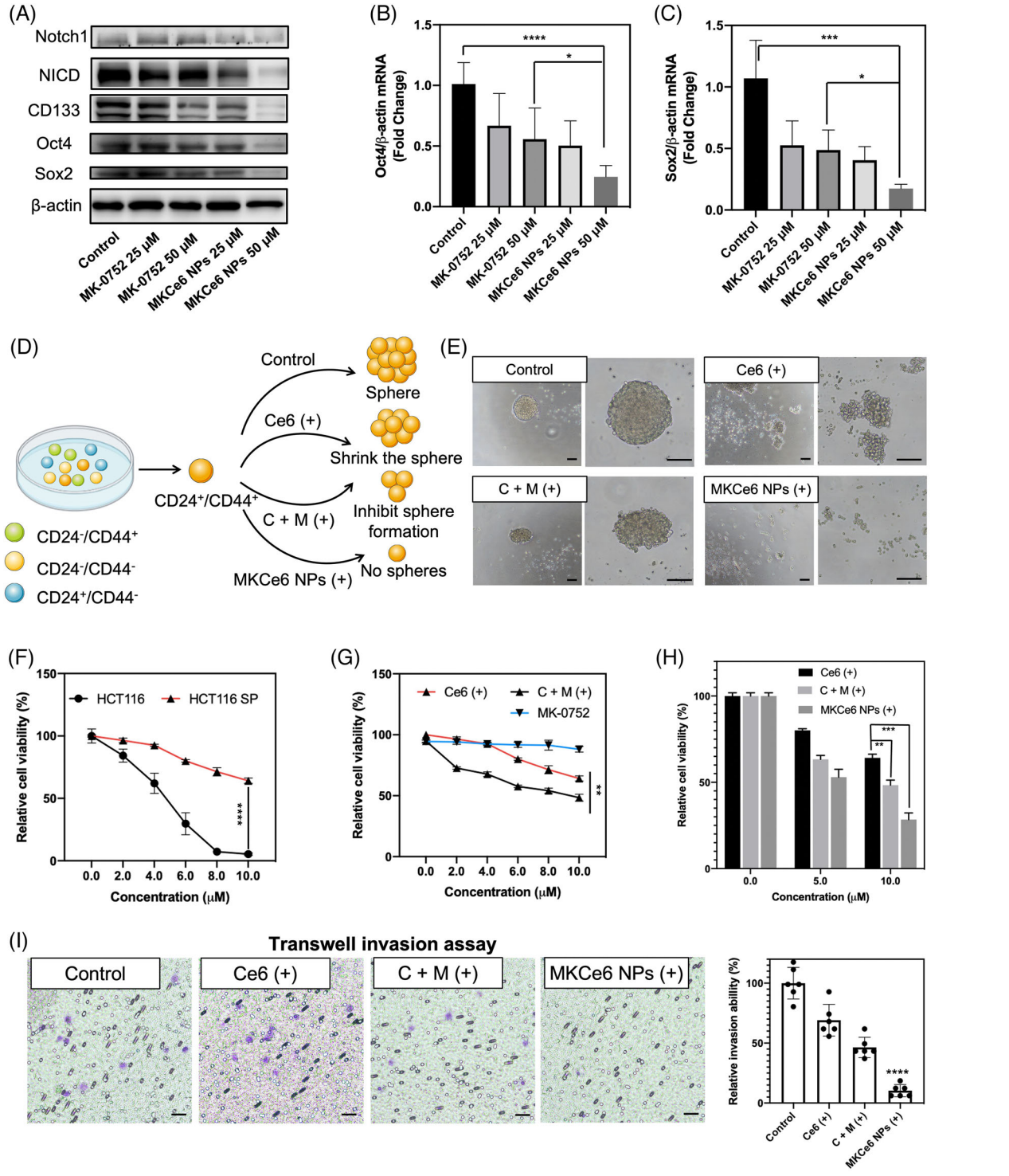

FIGURE 3 Stemness inhibition effect of MKCe6 nanoparticles (NPs) in vitro. (A) Western blot analysis of Notch1, NICD, CD133, Oct4, and Sox2 expression from HCT116 cells. The relative mRNA expression level of (B) Oct4 and (C) Sox2 in HCT116 cells after different treatments (n = 4). (D) Schematic illustration of the association between sphere formation and cell stemness with different treatments. (E) The representative images of tumorspheres formed by treated HCT116 cells over 7 days. Scale bar: 100 μm. (F) Cell viability of HCT116 cells and HCT116 SP cells after treatment with gradient concentrations of Ce6. (G) Cell viability of HCT116 SP cells after treatment with gradient concentrations of Ce6, MK-0752, and Ce6 plus MK-0752 (n = 3). (H) Cell viability of HCT SP 116 cells after treatment with gradient concentrations of Ce6, Ce6 plus MK-0725, and MKCe6 NPs together with light irradiation (n = 3). (I) The invasion ability testing of treated HCT116 cells with representative images and quantification of cells that invaded (n = 6). Scale bar: 200 μm. "(+)" represents the application of light irradiation. "C + M" represents the treatment of Ce6 plus MK-0752. Data were shown as mean ± SD. *p < 0.05, **p < 0.01, ***p < 0.001, ****p < 0.0001, and ns (not significant) were analyzed using Student's *t*-test

injected into the BALB/c nude mice bearing HCT116 tumors, they were visualized by an in vivo imaging system (IVIS) at 650 nm excitation wavelength at different time intervals. For the group treated with free Ce6, the fluorescence almost disappeared after 24 h, indicating fast metabolism of small molecules. However, the group treated with MKCe6 NPs exhibited increased fluorescence in a time-dependent manner, demonstrating prolong blood circulation and enhanced tumor accumulation (Figure 4A). Then the mice were sacrificed after 24 h. Major organs and tumors were harvested and

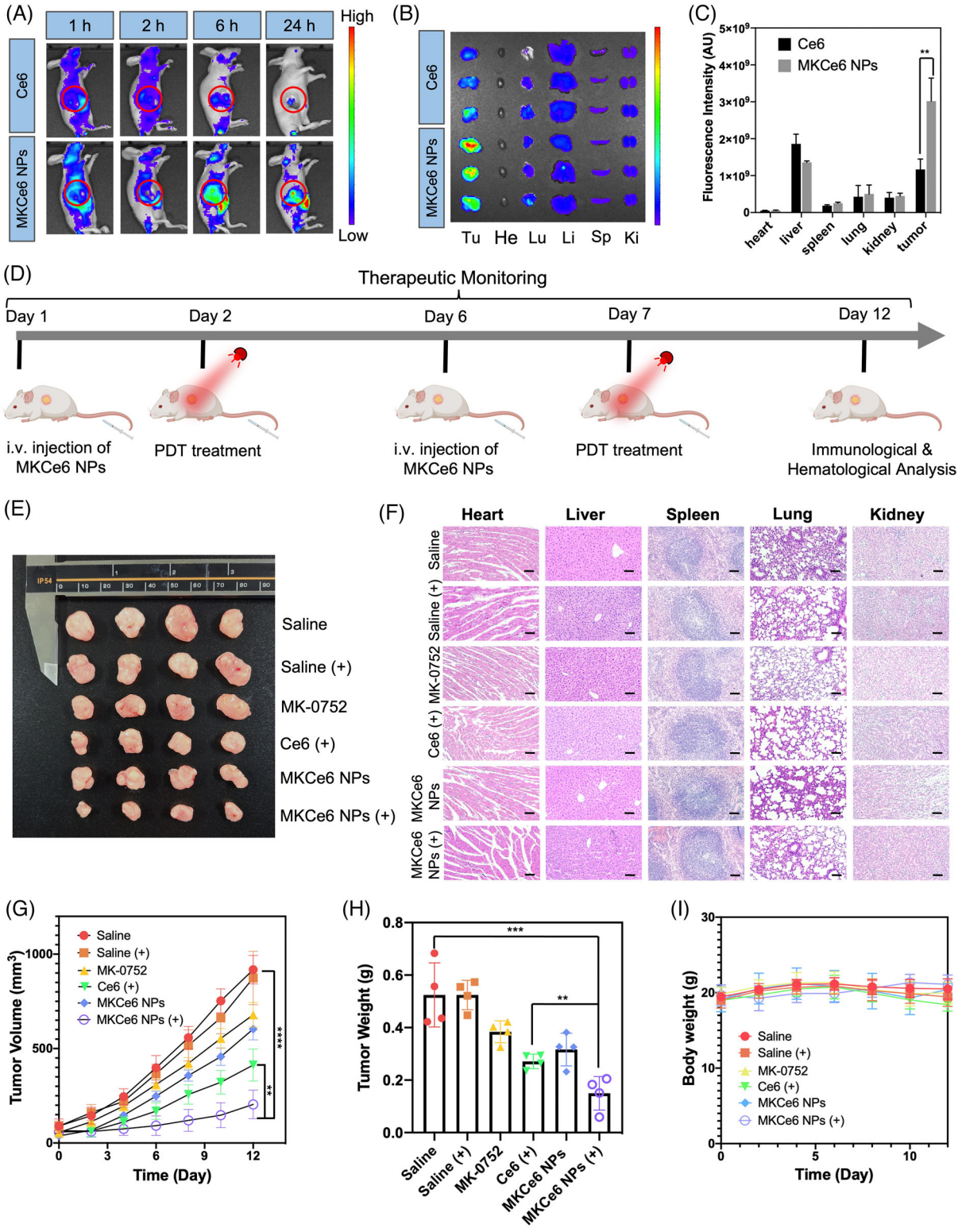

FIGURE 4 In vivo antitumor effect evaluation. (A) Biodistribution of Ce6 at different time intervals after intravenous injection of free Ce6 or MKCe6 nanoparticles (NPs). The tumors are indicated by red circles. (B) Ex vivo fluorescence images of major organs and tumors excised from the mice injected with free Ce6 and MKCe6 NPs. (C) Quantified fluorescence intensity of Ce6 in various organs determined from (B) (n = 3). (D) Therapeutic schedule with MKCe6 NPs for photodynamic therapy (PDT) and stemness inhibition against HCT116 subcutaneous tumors. (E) Photographs of the excised tumors after 12-day treatment in a subcutaneous colon cancer model. (F) Hematoxylin and eosin (H&E) staining of major organs including heart, liver, spleen, lung, and kidney from euthanized mice with different treatments. Scale bar: 200 μm. (G) Tumor volume, (H) tumor weight, and (I) body weight changes of the mice in the various treatment groups during the 12-day therapeutic period (n = 4). "(+)" represents the application of light irradiation. Data were shown as mean ± SD. *$p < 0.05$, **$p < 0.01$, ***$p < 0.001$, ****$p < 0.0001$, and ns (not significant) were analyzed using Student's *t*-test

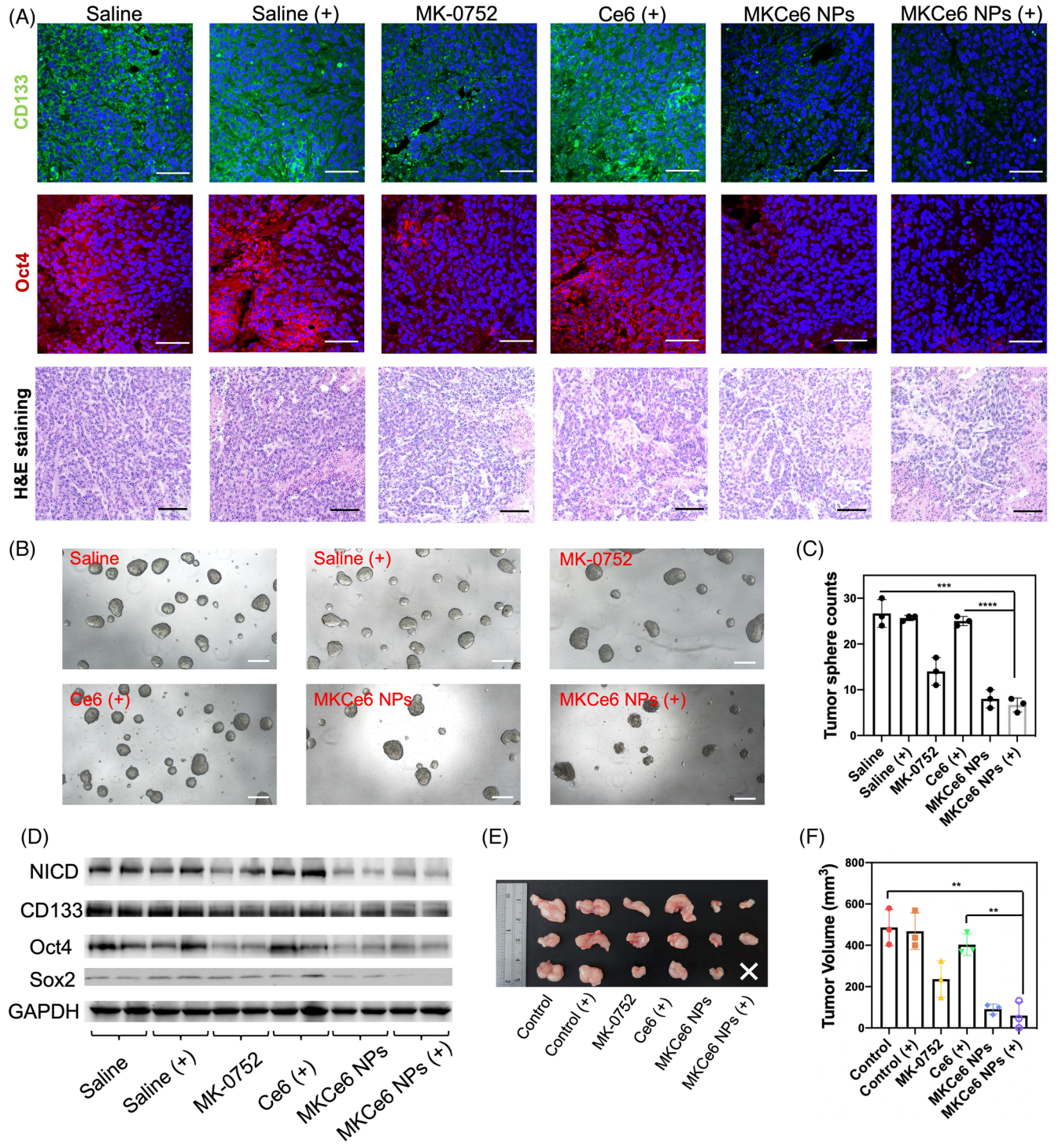

FIGURE 5 In vivo cancer stemness inhibition effect evaluation. (A) Hematoxylin and eosin (H&E) staining of tumor tissues in different treatment groups. Scale bar: 200 μm. CD133 and Oct4 expression levels of tumor tissues in different treatment groups were measured by immunofluorescence. All the nuclei were stained with 4′,6-diamidino-2-phenylindole (DAPI). Scale bar: 100 μm. (B) The tumorsphere formation of the isolated cancer cells from tumor tissues. Scale bar: 200 μm. (C) The isolated cancer cells were cultured in ultralow attachment dishes for 10 days, and the resultant spheres with a diameter over 50 μm were counted (n = 3). (D) Western blot analysis of NICD, CD133, Oct4, and Sox2 expression from isolated tumor tissues in different treatment groups. (E) Photograph and (F) volumes of the tumors of the mice 14 days post-inoculation of HCT116 SP cells with different treatments (n = 3). "(+)" represents the application of light irradiation. Data were shown as mean ± SD. *p < 0.05, **p < 0.01, ***p < 0.001, ****p < 0.0001, and ns (not significant) were analyzed using Student's *t*-test

visualized (Figure 4B,C). Compared with the group treated with free Ce6, MKCe6 NPs showed minimized accumulation in heart, liver, spleen, lung, and kidney, while distinct accumulation in tumors. The results guaranteed the biosafety and antitumor efficacy of the developed system.

The antitumor efficacy of MKCe6 NPs were evaluated in HCT116 tumor-bearing mice (Figure 4D, Figure S16). Six groups of mice were monitored over a period of different treatment. On day 12, tumor tissues were harvested and photographed (Figure 4E). Light irradiation alone could not inhibit the tumor growth, as indicated by the similar tumor growth rate compared to the saline-treated group. On the contrary, MKCe6 NPs plus light irradiation significantly inhibited tumor growth compared with the groups

treated with free Ce6 plus light irradiation. Moreover, the groups treated with free MK-0752 and MKCe6 NPs without light irradiation could also downregulate the rate of tumor growth, implying the inhibition of Notch signaling can inhibit tumor growth in certain degree (Figure 4E,G). The tumor weight also showed corresponding result, in which the tumors treated with MKCe6 NPs plus light exhibited the lowest weight (Figure 4H). Systemic toxicity of all formulations was not observed since negligible body weight change compared with the PBS group was seen (Figure 4I). Hematoxylin and eosin (H&E) staining on major organs (heart, liver, spleen, lung, and kidney) of mice for histological analysis revealed no apparent tissue damage in any organs after the treatments with the formulations (Figure 4F). Furthermore, analysis of key serum biochemical markers for the liver (alanine aminotransferase, ALT and aspartate transaminase, AST) showed no obvious systemic toxicity after the treatments (Figure S17).

2.7 | Intratumoral stemness inhibition in vivo

From the immunofluorescent results (Figure 5A), the tumor cells treated with MKCe6 NPs with or without light irradiation showed downregulated stemness protein expression compared to others, indicating the efficient intratumoral Notch signaling inhibition. However, only the group treated with MKCe6 NPs under NIR light irradiation exhibited serious damage the tumor tissue as revealed by H&E staining results (Figure 5A), implying that stemness inhibition-enhanced PDT can achieve the best antitumor efficacy.

To further confirm intratumoral stemness inhibition effects, fresh tumors in different treatment groups were isolated and single tumor cell suspension were obtained to test the tumorsphere formation capability. As shown in Figure 5B,C, the groups treated with MKCe6 NPs exhibited dampened tumorsphere formation. Moreover, proteins were extracted from the tumors shown in Figure 4E and the stemness-related protein expression was measured using western blot assay. Similar results were drawn that the group treated with MKCe6 NPs displayed remarkable protein downregulation with or without light irradiation (Figure 5D).

Given the impaired cancer stemness, we thus assumed that the tumorigenicity, a key feature tightly associated with cancer stemness, would be reduced accordingly in remaining cancer cells.[46] To test this, HCT116 SP cells were sorted out and cultured with different treatments in vitro. Then survived HCT116 SP cells in different treated groups were subcutaneously inoculated into nude mice. Notably the groups treated with MKCe6 NPs formed new tumor mass with much lower efficiency than other groups (Figures 5E,F, S18, and S19). These observations revealed the impaired tumorigenic capability of MKCe6 NPs-treated cells, suggesting a reduced risk of tumor recurrence.

3 | CONCLUSION

A drug delivery system, self-assembled by Ce6 and MK-0752, by virtue of π-π stacking, hydrophobic, and electrostatic interactions was successfully constructed to achieve stemness inhibition-enhanced PDT. The stemness inhibition could synergize PDT toward a better anticancer efficacy by simultaneously targeting both differentiated and undifferentiated cancer cells. The stability, solubility, and biocompatibility of MKCe6 NPs were improved compared with free molecules. The carrier-free MKCe6 NPs possessed a high drug-loading capacity and evaded the potential immunogenicity from extra carriers. In vitro and in vivo results demonstrated the feasibility of MKCe6 NPs for both cancer stemness modulation and tumor growth inhibition with less tumorigenesis potential, showing the potency as advanced therapeutics for cancer therapy with high efficacy and low systemic side effects.

ACKNOWLEDGMENTS

This work was supported by the Research Grants Council of Hong Kong (Early Career Scheme, No. 27115220) and Ming Wai Lau Centre for Reparative Medicine Associate Member Program. We acknowledge the assistance of the Faculty Core Facility of Li Ka Shing Faculty of Medicine, The University of Hong Kong.

CONFLICT OF INTEREST

The authors declare no conflict of interest.

DATA AVAILABILITY STATEMENT

All the data supporting the findings of this study are available within the article and its Supporting Information files, and from the corresponding author on request.

ETHICS STATEMENT

All animals received care and experiments according to the protocol that was evaluated and approved by the Committee on the Use of Live Animals in Teaching and Research (CULATR) at The University of Hong Kong (CULATR No. 5827-21).

ORCID

Weiping Wang https://orcid.org/0000-0001-7511-3497

REFERENCES

1. N. M. Akella, G. Le Minh, L. Ciraku, A. Mukherjee, Z. A. Bacigalupa, D. Mukhopadhyay, V. L. Sodi, M. J. Reginato, *Mol. Cancer Res.* **2020**, *18*, 585.
2. K. Eun, S. W. Ham, H. Kim, *BMB Rep.* **2017**, *50*, 117.
3. H. Clevers, *Nat. Med.* **2011**, *17*, 313.
4. N. K. Lytle, A. G. Barber, T. Reya, *Nat. Rev. Cancer* **2018**, *18*, 669.
5. Y. Li, H. A. Rogoff, S. Keates, Y. Gao, S. Murikipudi, K. Mikule, D. Leggett, W. Li, A. B. Pardee, C. J. Li, *Proc. Nat. Acad. Sci. U.S.A.* **2015**, *112*, 1839.
6. F. Islam, V. Gopalan, R. A. Smith, A. K. Lam, *Exp. Cell Res.* **2015**, *335*, 135.
7. H. Kahroba, M. Shirmohamadi, M. S. Hejazi, N. Samadi, *Life Sci.* **2019**, *239*, 116986.
8. C. R. Arnold, J. Mangesius, I.-I. Skvortsova, U. Ganswindt, *Front. Oncol.* **2020**, *10*, 164.
9. M. Najafi, K. Mortezaee, J. Majidpoor, *Life Sci.* **2019**, *234*, 116781.
10. L. T. H. Phi, I. N. Sari, Y. G. Yang, S. H. Lee, N. Jun, K. S. Kim, Y. K. Lee, H. Y. Kwon, *Stem. Cells Int.* **2018**, *2018*, 5416923.
11. T. Huang, X. Song, D. Xu, D. Tiek, A. Goenka, B. Wu, N. Sastry, B. Hu, S. Y. Cheng, *Theranostics* **2020**, *10*, 8721.
12. L. Seguin, J. S. Desgrosellier, S. M. Weis, D. A. Cheresh, *Trends Cell Biol.* **2015**, *25*, 234.

13. N. K. Lytle, L. P. Ferguson, N. Rajbhandari, K. Gilroy, R. G. Fox, A. Deshpande, C. M. Schürch, M. Hamilton, N. Robertson, W. Lin, P. Noel, M. Wartenberg, I. Zlobec, M. Eichmann, J. A. Galván, E. Karamitopoulou, T. Gilderman, L. A. Esparza, Y. Shima, P. Spahn, R. French, N. E. Lewis, K. M. Fisch, R. Sasik, S. B. Rosenthal, M. Kritzik, D. Von Hoff, H. Han, T. Ideker, …, T. Reya, *Cell* **2019**, *177*, 572. e22.
14. H. E. Lee, J. H. Kim, Y. J. Kim, S. Choi, S. Kim, E. Kang, I. Chung, I. Kim, E. Kim, Y. Choi, *Br. J. Cancer* **2011**, *104*, 1730.
15. X. Yuan, H. Wu, N. Han, H. Xu, Q. Chu, S. Yu, Y. Chen, K. Wu, *J. Hematol. Oncol.* **2014**, *7*, 87.
16. E. V. Abel, E. J. Kim, J. Wu, M. Hynes, F. Bednar, E. Proctor, L. Wang, M. L. Dziubinski, D. M. Simeone, *PLoS One* **2014**, *9*, e91983.
17. P. C. Tien, M. Quan, S. Kuang, *Cancer Lett.* **2020**, *494*, 27.
18. L. Y. Jiang, X. L. Zhang, P. Du, J. H. Zheng, *Chin. J. Cancer Res.* **2011**, *23*, 140.
19. P. Bu, K. Y. Chen, J. H. Chen, L. Wang, J. Walters, Y. J. Shin, J. P. Goerger, J. Sun, M. Witherspoon, N. Rakhilin, J. Li, H. Yang, J. Milsom, S. Lee, W. Zipfel, M. M. Jin, Z. H. Gümüş, S. M. Lipkin, X. Shen, *Cell Stem. Cell* **2013**, *12*, 602.
20. S. M. McAuliffe, S. L. Morgan, G. A. Wyant, L. T. Tran, K. W. Muto, Y. S. Chen, K. T. Chin, J. C. Partridge, B. B. Poole, K. H. Cheng, J. Daggett, Jr., K. Cullen, E. Kantoff, K. Hasselbatt, J. Berkowitz, M. G. Muto, R. S. Berkowitz, J. C. Aster, U. A. Matulonis, D. M. Dinulescu, *Proc. Nat. Acad. Sci. U.S.A.* **2012**, *109*, E2939.
21. C. Giovannini, M. Baglioni, M. Baron Toaldo, C. Ventrucci, S. D'Adamo, M. Cipone, P. Chieco, L. Gramantieri, L. Bolondi, *Oncotarget* **2013**, *4*, 1618.
22. X. Li, J. F. Lovell, J. Yoon, X. Chen, *Nat. Rev. Clin. Oncol.* **2020**, *17*, 657.
23. H. O. Alsaab, M. S. Alghamdi, A. S. Alotaibi, R. Alzhrani, F. Alwuthaynani, Y. S. Althobaiti, A. H. Almalki, S. Sau, A. K. Iyer, *Cancers* **2020**, *12*, 2793.
24. J. Xie, Y. Wang, W. Choi, P. Jangili, Y. Ge, Y. Xu, J. Kang, L. Liu, B. Zhang, Z. Xie, J. He, N. Xie, G. Nie, H. Zhang, J. S. Kim, *Chem. Soc. Rev.* **2021**, *50*, 9152.
25. M. F. Wei, M. W. Chen, K. C. Chen, P. J. Lou, S. Y. Lin, S. C. Hung, M. Hsiao, C. J. Yao, M. J. Shieh, *Autophagy* **2014**, *10*, 1179.
26. J. Morgan, J. D. Jackson, X. Zheng, S. K. Pandey, R. K. Pandey, *Mol. Pharm.* **2010**, *7*, 1789.
27. Z. G. Movahed, M. Rastegari-Pouyani, M. hossein Mohammadi, K. Mansouri, *Biomed. Pharmacother.* **2019**, *112*, 108690.
28. I. Krop, T. Demuth, T. Guthrie, P. Y. Wen, W. P. Mason, P. Chinnaiyan, N. Butowski, M. D. Groves, S. Kesari, S. J. Freedman, *J. Clin. Oncol.* **2012**, *30*, 2307.
29. I. Krop, T. Demuth, T. Guthrie, P. Y. Wen, W. P. Mason, P. Chinnaiyan, N. Butowski, M. D. Groves, S. Kesari, S. J. Freedman, S. Blackman, J. Watters, A. Loboda, A. Podtelezhnikov, J. Lunceford, C. Chen, M. Giannotti, J. Hing, R. Beckman, P. Lorusso, *J. Clin. Oncol.* **2012**, *30*, 2307.
30. L. Sun, Q. Li, M. Hou, Y. Gao, R. Yang, L. Zhang, Z. Xu, Y. Kang, P. Xue, *Biomater. Sci.* **2018**, *6*, 2881.
31. Y. Liu, M. He, R. Guo, Z. Fang, S. Kang, Z. Ma, M. Dong, W. Wang, L. Cui, *Appl. Catal. B* **2020**, *260*, 118137.
32. J. Wei, J. Li, D. Sun, Q. Li, J. Ma, X. Chen, X. Zhu, N. Zheng, *Adv. Funct. Mater.* **2018**, *28*, 1706310.
33. Y. Nakamura, A. Mochida, P. L. Choyke, H. Kobayashi, *Bioconjugate Chem.* **2016**, *27*, 2225.
34. J. Fang, W. Islam, H. Maeda, *Adv. Drug. Deliv. Rev.* **2020**, *157*, 142.
35. Y. S. Nam, T. Shin, H. Park, A. P. Magyar, K. Choi, G. Fantner, K. A. Nelson, A. M. Belcher, *J. Am. Chem. Soc.* **2010**, *132*, 1462.
36. J. Rejman, V. Oberle, I. S. Zuhorn, D. Hoekstra, *Biochem. J.* **2004**, *377*, 159.
37. C. T. Jordan, M. L. Guzman, M. Noble, *N. Engl. J. Med.* **2006**, *355*, 1253.
38. L. Walcher, A. K. Kistenmacher, H. Suo, R. Kitte, S. Dluczek, A. Strauß, A. R. Blaudszun, T. Yevsa, S. Fricke, U. Kossatz-Boehlert, *Front. Immunol.* **2020**, *11*, 1280.
39. T. R. McCaw, E. Inga, H. Chen, R. Jaskula-Sztul, V. Dudeja, J. A. Bibb, B. Ren, J. B. Rose, *Oncologist* **2021**, *26*, e608.
40. I. Ben-Porath, M. W. Thomson, V. J. Carey, R. Ge, G. W. Bell, A. Regev, R. A. Weinberg, *Nat. Genet.* **2008**, *40*, 499.
41. S. K. Nicolis, *Neurobiol. Dis.* **2007**, *25*, 217.
42. D. Horst, L. Kriegl, J. Engel, T. Kirchner, A. Jung, *Br. J. Cancer* **2008**, *99*, 1285.
43. J. Tang, H. Zhou, J. Liu, J. Liu, W. Li, Y. Wang, F. Hu, Q. Huo, J. Li, Y. Liu, C. Chen, *ACS Appl. Mater. Interfaces* **2017**, *9*, 23497.
44. E. K. Kim, J. H. Cho, E. Kim, Y. J. Kim, *PLoS One* **2017**, *12*, e0181183.
45. A. Jaggupilli, E. Elkord, *Clin. Dev. Immunol.* **2012**, *2012*, 708036.
46. M. Todaro, F. Iovino, V. Eterno, P. Cammareri, G. Gambara, V. Espina, G. Gulotta, F. Dieli, S. Giordano, R. De Maria, *Cancer Res.* **2010**, *70*, 8874.

SUPPORTING INFORMATION

Additional supporting information can be found online in the Supporting Information section at the end of this article.

How to cite this article: Y. Liu, K. Long, T. Wang, W. Kang, W. Wang, *Aggregate* **2023**, *4,* e284. https://doi.org/10.1002/agt2.284